Increase in terahertz-wave generation by difference frequency mixing by the overlap of exciton states in different GaAs/AlAs quantum wells and spectroscopic measurements

Sakaue, Kanta

Kojima, Osamu

Kita, Takashi

Steer, Matthew J.

Hogg, Richard A.

(Citation)
Optics Express,29(15):24387-24395

(Issue Date)
2021-07-19

(Resource Type)
journal article

(Version)
Version of Record

Research Article | Vol. 29, No. 15 / 19 July 2021 / Optics Express 24387
Optics EXPRESS

Increase in terahertz-wave generation by difference frequency mixing by the overlap of exciton states in different GaAs/AlAs quantum wells and spectroscopic measurements

KANTA SAKAUE,[1] OSAMU KOJIMA,[1,*] TAKASHI KITA,[1] MATTHEW J. STEER,[2] AND RICHARD A. HOGG[2]

[1]Department of Electrical and Electronic Engineering, Graduate School of Engineering, Kobe University, 1-1 Rokkodai, Nada, Kobe 657-8501, Japan
[2]Electronics and Nanoscale Engineering, James Watt School of Engineering, University of Glasgow, Glasgow G12 8LT, United Kingdom
[*]kojima@phoenix.kobe-u.ac.jp

Abstract: Intense terahertz-wave emission in the higher frequency region can result in various applications such as terahertz spectroscopy and ultrafast data communication. In this study, an increase in terahertz waves by the overlap of exciton states in different quantum wells and spectroscopic demonstration are reported. The excitation energy dependence of signal intensity shows the effect of the overlap. The signals measured under the condition of square dependence of intensity on the excitation power indicate interference with the periods corresponding to the laser energy difference. Furthermore, the absorption coefficient of the transparent sheet is obtained at specific frequency. These results indicate that the generation of intense terahertz waves at various frequencies using excitons is possible and that difference frequency mixing is a useful terahertz-wave source.

1. Introduction

Various applications of terahertz (THz) waves have been proposed, e.g., gas and virus sensing [1–4], THz scanners [5–7], and ultra-high-speed optical communication [8–10]. A monocycle THz-wave pulse with a broad peak bandwidth of approximately 1 THz generated by ultrashort pulse lasers has been mainly used for THz spectroscopy [11–13]. In this case, the spectral bandwidth of THz waves and the spectroscopic resolution are strongly related to the laser pulse width, scanning step, and moving length. Furthermore, this type of signal is obtained by the time-domain measurement; thus, a Fourier transform is required to obtain information in the frequency domain.

In contrast, we focused on THz spectroscopy systems that are based on the difference frequency mixing (DFM) process using two external lasers [14,15]. For the DFM process, the bandwidth and frequency of generated THz waves are decided by the excitation laser spectral widths and energy difference; thus, the DFM process is a good method for the generation of THz waves at various frequencies with fine resolution. In addition, it is possible to obtain the frequency-domain information without a Fourier transform. The intensity of THz waves generated by the DFM process using a photoconductive antenna, which has been the main method, considerably decreases owing to phonon scattering at frequencies higher than 2 THz [16,17]. In contrast, the use of excitons confined in quantum wells (QWs) allows to generate THz waves in a wider frequency range [14,15]. However, in previous reports, strong emission was limited around the heavy-hole (HH) exciton energy of QW. Considering the application of the exciton-based THz-wave system to spectroscopy, the generation of strong THz waves in a wide frequency range is essential. For instance, in the case of the third optical nonlinear polarizations, the

#431329 https://doi.org/10.1364/OE.431329
Journal © 2021 Received 12 May 2021; revised 7 Jul 2021; accepted 7 Jul 2021; published 16 Jul 2021

Optics EXPRESS

nonlinear signals were enhanced at the LH excitons in the low temperature [18,19]. In addition, the simultaneous excitation is very similar to the generation scheme of the exciton quantum beat. In the case of the quantum beat of HH and LH excitons, the simultaneous excitation leads to the maximum intensity [20–23]. Therefore, the enhancement of THz signal intensity due to DFM by excitation of HH and LH excitons was expected. However, the spectrally resolved signals showed that the exciton dephasing decreases the intensity of the nonlinear process [24]. Hence, we considered, because the ionization of LH exciton and the intersubband transition from LH to HH decreases the number of LH excitons and the overlap of HH and LH excitons is weakened, the second nonlinear polarization is suppressed. Therefore, in this study, to widely increase the intensity of the THz wave, the THz intensity is assisted by the HH exciton in QWs with different thicknesses. The overlap effects of two exciton states on the THz-wave intensity were observed. The THz signal is discussed on the basis of the excitation power dependence and frequency measurements. Furthermore, the basic spectroscopic result is demonstrated.

2. Experiment

In this study, three samples were used, which consisted of undoped GaAs/AlAs multiple QWs (MQWs) embedded in a p-i-n structure on a (001) GaAs substrate grown by molecular beam epitaxy. The sample structures are schematically shown in Figs. 1(a), 1(b), and 1(c). The surface p-doped GaAs layer with a doping concentration of 1×10^{18} cm^{-3} has 50 nm thickness, and the n-doped GaAs buffer layer with a doping concentration of 3×10^{18} cm^{-3} has 1500 nm thickness. The GaAs and AlAs thickness of the first MQW sample is 7.25 nm, 7.25/7.25, and the MQW period is 30. The details of this sample was reported in the Ref. [24]. The second MQWs sample consists of 7.25/7.25 MQW with 11 periods, 6.67/6.67 MQW with 11 periods, and 6.09/6.09 MQW with 11 periods from the substrate side. The third MQW sample also consists of three MQWs: 7.25/7.25 MQW with 12 periods, 6.38/6.38 MQW with 11 periods, and 5.51/5.51 MQW with 11 periods. The internal electric field estimated from the doping concentration is 16.0 kV/cm. Hereafter, these samples are called A, B, and C, respectively. The photoluminescence (PL) spectra to evaluate exciton energies are shown in Fig. 1(d). HH and LH excitons in 7.25/7.25 MQW are labeled as HHA and LHA, respectively. All samples include 7.25/7.25 MQW; thus, the notations of HHA and LHA are commonly used. In sample B, HH exciton (HHB) in 6.67/6.67 MQW is located between HHA and LHA, and HH exciton in 6.38/6.38 MQW of sample C (HHC) is close to LHA.

In the measurement of the DFM signal, two semiconductor lasers (L830H as L_1 and L808P200 as L_2) were used. The energy of L_1 was chosen to excite HHA, and the energy of L_2 was changed around the LHA energy from 1.5287 to 1.5412 eV. The experimental setup is schematically shown in Fig. 1(e). Two laser beams were combined by an optical fiber coupler, and the combined beam was focused on the sample surface through a hole in the off-axis parabolic mirror by a polymethylpentene lens, which was also used to collimate the emitted THz wave. A Si wafer was used to eliminate the contribution of laser light to the signal. Excitation power was controlled by a variable neutral-density filter. The frequency of THz waves can be measured with a Fabry–Perot interferometer, which consists of two silicon wafers, as shown in Fig. 1(f). The THz signal was detected by a pyroelectric sensor and amplified by a lock-in-amplifier at 5 Hz. All measurements were performed at 297 K. The excitation power dependence of signal intensity was measured under a humidity of less than 60%, and the excitation energy dependence was measured under a humidity of 10%.

Optics EXPRESS

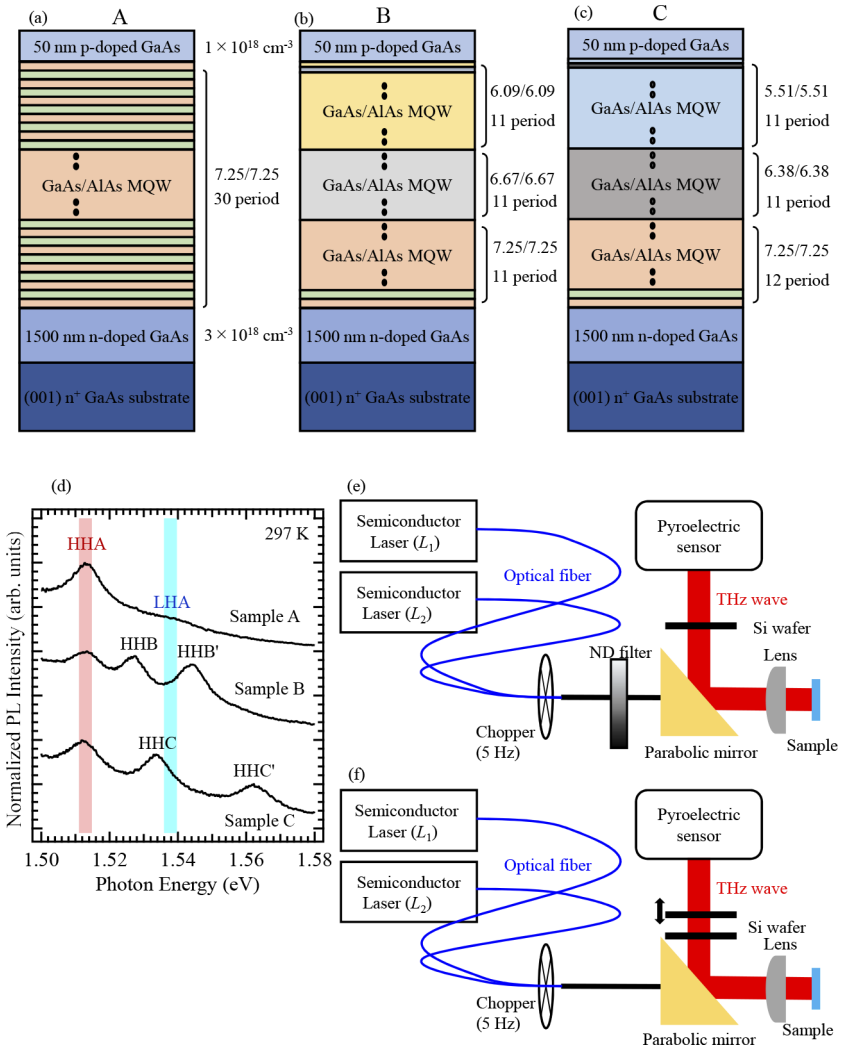

Fig. 1. (a)-(c)Schematics of the sample structures. The samples of B and C consists of three MQWs, as shown in (b) and (c). (d) The PL spectra of the samples. The experimental setups for (e) excitation-power dependence and excitation-energy dependences and (f) Fabry-Perot interferometer for frequency measurement.

Optics EXPRESS

3. Results and discussion

Figure 2(a) shows the dependence of the signal intensity on the L_2 energy measured at various excitation powers. The lower horizontal axis represents the frequency converted from the energy difference between L_1 and L_2 energies, which is shown as the upper horizontal axis. The circles, triangles, and squares indicate signal intensities in samples A, B, and C, respectively. On the basis of our previous results [14,15], the signals can be classified into three regions: (i) large contribution of the heat radiation owing to carrier-phonon interaction to the signal (12 mW), (ii) mainly owing to the THz wave (21 mW), and (iii) originating from saturated second nonlinear polarization (30 mW).

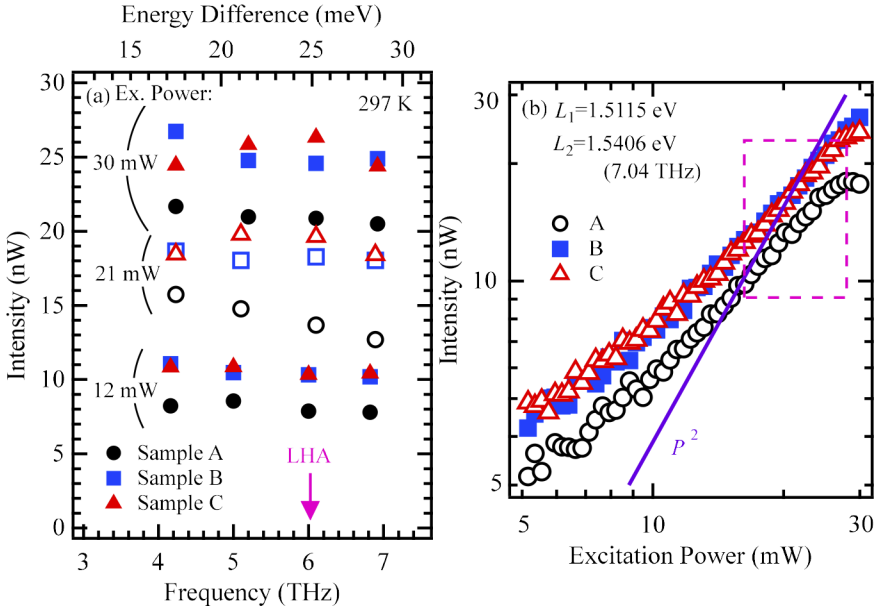

Fig. 2. (a) Signal intensities measured by various L_2 energies and laser powers. The circles, squares, and triangles show the results of samples A, B, and C, respectively. The arrow indicates the LHA energy. (b) The excitation power dependence of the signals. The circles, squares, and triangles show the experimental results observed in samples A, B, and C, respectively. Laser energies were tuned to 1.5115 and 1.5406 eV, whose energy difference corresponds to 7.04 THz. Solid line indicates the gradient of square dependence for the excitation power. In the dotted square, signal intensities demonstrate the square dependence.

At first, the results in sample A (circles) are discussed. This sample includes only 7.25/7.25 MQW that is contained in all samples. At weak excitation power, the signal intensity hardly changes by excitation energy owing to the contribution of heat caused by the carrier-phonon interaction to the signal. In contrast, at larger excitation power, the signal intensity depends on excitation energy, and the intense signal at approximately 4 THz is attributed to the inhomogeneous width of HHA. However, when the second-order nonlinear optical effect is saturated, the energy dependence is weakened.

For samples B (squares) and C (triangles), the dependence of intensity on excitation energy differs from the results for sample A. At lower excitation power, although the intensities are larger than those in sample A, the excitation energy dependence is not clear. In contrast, when excitation power increases, signal intensity increases, and the excitation energy dependence exhibits unique profiles. Specifically, a peak appears at the LHA energy in sample C and the conversion efficiency at the peak is 2.92×10^{-3}%. To convert the signal intensity to the power, we only considered

Optics EXPRESS

the frequency dependence of the sensitivity of the sensor, and in this frequency region, the detector has an almost constant sensitivity. Therefore, this dependence does not originate from the frequency dependence of sensitivity, and this increase in signal intensity originates from the stack of MQWs; HHB and HHC on LHA.

The intensity of signals based on second nonlinear polarizations, as well DFM signals, exhibits square dependence on the excitation power. Thus, the details of excitation power dependence were measured, as shown in Fig. 2(b). In these measurements, the lasers were tuned to HHA and LHA energies. The dotted line indicates the gradient of the square dependence. With an increase in the excitation power, signal intensities linearly increase at weaker excitation power and exhibit square dependence in stronger power region (dotted square region) for all samples. Therefore, the signals observed at the excitation powers of 21 and 30 mW shown in Fig. 2(a) originate from the THz wave for all samples. In Supplement 1, Fig. S1 shows that square dependence was observed under other frequency conditions.

The THz-wave frequency can be evaluated by interference signals measured with a Fabry–Perot interferometer. Then, the frequencies under strong signal conditions in sample C were measured, as shown in Figs. 3(a) and 3(b), where the laser power was 30 mW. The laser spectra used are shown in the insets. The frequencies converted from the energy difference of two laser peaks, which were obtained by the Gaussian fitting of the laser spectra, are 5.34 THz in Fig. 3(a) and 7.04 THz in Fig. 3(b). The interference signals were fitted with a sine function, and the fitting results are shown as solid curves. The period evaluated by fitting in Fig. 3(a) is 28.15 ± 0.82 μm, which corresponds to 5.33 ± 0.15 THz. Furthermore, the signal period in Fig. 3(b) is 29.47 ± 1.58 μm, which corresponds to 7.04 ± 0.37 THz in Fig. 3(b). Therefore, THz signal can be enhanced by the overlap of two exciton states, such as in samples B and C, which is the key point of this study.

Here, an increase in intensity assisted by HHB and HHC is discussed. As mentioned above, LHA rapidly disappears owing to the intersubband transition from LH to HH states at room temperature; thus, the overlap of LHA and HHA, which creates nonlinear polarization emitting THz waves, is small. In contrast, for stacked MQW samples, the signal intensity increased owing to HH excitons in different MQW. Although LHA is spatially apart from HHB and HHC, the signals were enhanced. To explain this point, there are two possible factors, i.e., the resonant effects and the larger radius of the second nonlinear polarization. In samples B and C, LHA is located in the inhomogeneous broadening width of HHB and near HHC, respectively. Here, the tunneling from HH to LH is not a major factor. The relationship of calculated confinement energies is illustrated in Supplement 1, Fig. S2. In samples B and C, the HH states in 6.67/6.67 and 6.38/6.38 QWs are close to LH in 7.25/7.25 QW. However, 7.25/7.25 MQW is located on the n-side. Therefore, the hole movement is toward the n-side; the hole transition from 6.67/6.67 and 6.38/6.38 QWs to 7.25/7.25 QW is difficult. The PL spectra measured by the resonant excitation of HHB and HHC are shown in Figs. 4(a) and 4(b), respectively. When HH of HHB and HHC transfers to the LH state in 7.25/7.25 QW, strong HHA PL owing to the intersubband transition from the LH state should appear. However, HHA PL is hardly observed in Figs. 4(a) and 4(b). Therefore, tunneling from HH to LH does not contribute to an increase in intensity at the LHA energy.

Then, we considered that the second nonlinear polarization has a larger radius. As illustrated in Supplement 1, Fig. S3, at the interface around 6.38/6.38 MQW and 7.25/7.25 MQW in sample C, the positions of two excitons, HHA and HHC, are very close. When those generate second nonlinear polarization as a complex of two excitons owing to the weak coupling, the radius is larger than the barrier width. This large radius enables the overlap of two excitons that are spatially separated by the barrier layer.

Finally, we demonstrate spectroscopic measurements using our DFM process. Commercial overhead-projector (OHP) sheets with a thickness of 0.106 ± 0.005 mm were used as samples.

Optics EXPRESS

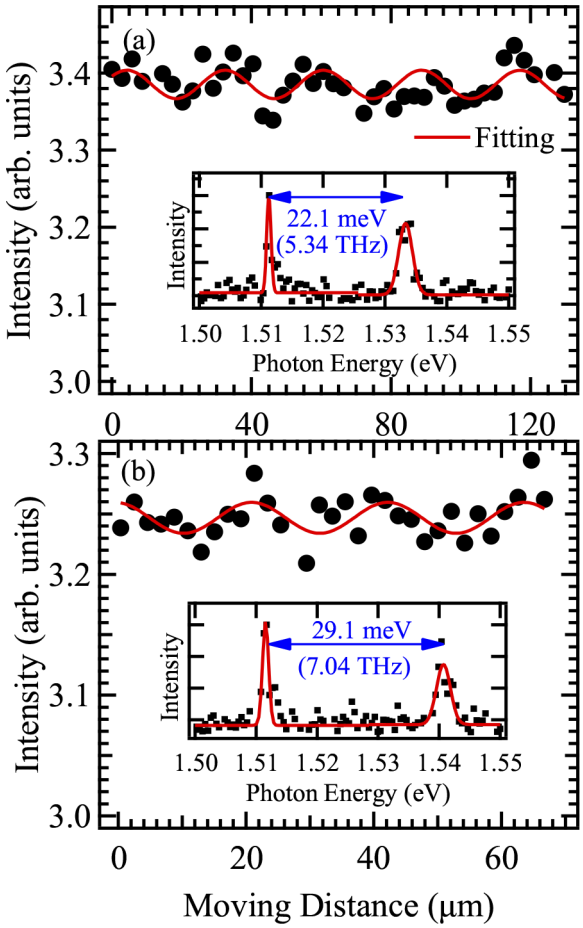

Fig. 3. Interference signals measured by a Fabry-Perot interferometer with the calculated frequencies of 5.34 (a) and 7.04 (b) THz. Solid curves show the fitting results by a sine function. The insets show the laser spectra.

Figure 5(a) demonstrates the thickness dependence of signal intensity through the sheets, where the thickness was changed by an increase in the number of sheets. In this measurement, the frequency was 7.03 THz. Intensity decreases with an increase in thickness, which demonstrates the absorption measurement. This result was fitted with a function of $I(d) = I_0 e^{-\alpha d}$, where d is the thickness, I_0 is the intensity without sheets, and α is the absorption coefficient at 7.03 THz, as shown by the solid curve. Using this fitting, the absorption coefficient of 30.46 cm^{-1} was obtained. Considering the Fourier transform infrared (FTIR) spectrum in Fig. 5(b), which was measured by FT/IR-430 (JASCO), the value seems to be reasonable. In contrast, the absorption in Fig. 5(a) has a baseline, which results from blackbody effects caused by carrier-carrier scattering, carrier-phonon scattering, and so on. This baseline due to the thermal effect was observed as the linear dependence components in the results of the excitation-power dependences in Fig. 2(b) and Supplement 1, Fig. S1. Therefore, the suppression of this baseline will make the system more useful.

Optics EXPRESS

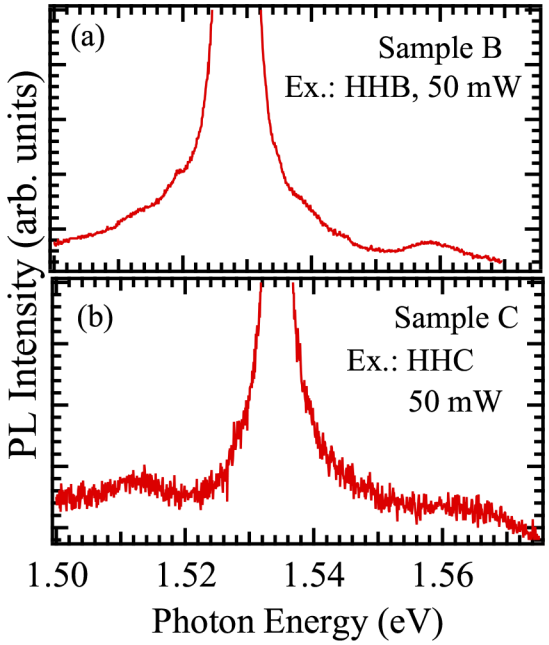

Fig. 4. PL spectra measured by the resonant excitation of HHB (a) and HHC (b).

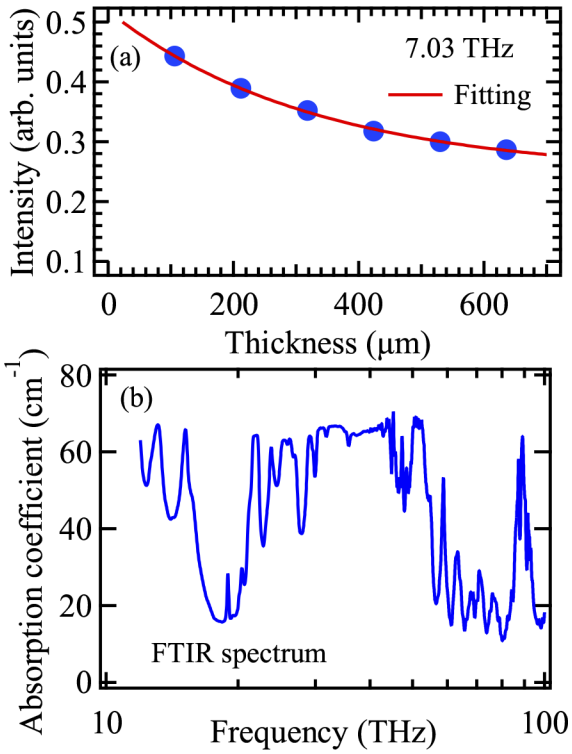

Fig. 5. (a) Absorption measurement using OHP sheets measured at the 7.03 THz condition. The horizontal axis is given as the product of the number of sheets and sheet thickness. The solid curve is a fitting curve. (b) Fourier transform infrared spectrum of the absorption coefficient. The horizontal axis is indicated by the logarithmic scale.

Optics EXPRESS

4. Conclusion

We investigated the effects of overlap of exciton states in multiply stacked MQWs on the DFM signal intensity. The overlap of HH exciton on LH exciton shows an increase in the THz-wave intensity, such as the overlap of HHC on LHA. On the basis of the results of resonant PL, the weak coupling of two spatially separated excitons causes second nonlinear polarization with a larger radius, which emits the THz wave. Furthermore, the evaluated value of the absorption coefficient of the OHP sheet demonstrated a reasonable value that was comparable with that obtained by the FTIR measurement. Therefore, the energetical overlap of exciton states can increase the THz-wave intensity, and DFM will allow THz-wave sensing.

Funding. Hyogo Foundation for Science and Technology; Support Center for Advanced Telecommunications Technology Research Foundation; Kawanishi Memorial ShinMaywa Education Foundation; Sasakura Enviro-Science Foundation; JSPS International Research Fellow; Japan Society for the Promotion of Science (KAKENHI 16KK0129, 19K04532, 26289088).

Acknowledgments. The author would like to thank Enago for the English language review.

Disclosures. The authors declare no conflicts of interest.

Data availability. Data underlying the results presented in this paper are not publicly available at this time but may be obtained from the authors upon reasonable request.

Supplemental document. See Supplement 1 for supporting content.

References

1. D. M. Mittleman, R. H. Jacobsen, R. Neelamani, R. G. Baraniuk, and M. C. Nuss, "Gas sensing using terahertz time-domain spectroscopy," Appl. Phys. B: Lasers Opt. **67**(3), 379–390 (1998).
2. B. You and J.-Y. Lu, "Sensitivity analysis of multilayer microporous polymer structures for terahertz volatile gas sensing," Opt. Express **25**(5), 5651–5661 (2017).
3. S. J. Park, S. H. Cha, G. A. Shin, and Y. H. Ahn, "Sensing viruses using terahertz nano-gap metamaterials," Biomed. Opt. Express **8**(8), 3551–3558 (2017).
4. K. Shih, P. Pitchappa, L. Jin, C.-H. Chen, R. Singh, and C. Lee, "Nanofluidic terahertz metasensor for sensing in aqueous environment," Appl. Phys. Lett. **113**(7), 071105 (2018).
5. H. Chen, T.-H. Chen, T.-F. Tseng, J.-T. Lu, C.-C. Kuo, S.-C. Fu, W.-J. Lee, Y.-F. Tsai, Y.-Y. Huang, E. Y. Chuang, Y.-J. Hwang, and C.-K. Sun, "High-sensitivity *in vivo* THz transmission imaging of early human breast cancer in a subcutaneous xenograft mouse model," Opt. Express **19**(22), 21552–21562 (2011).
6. D. Suzuki, S. Oda, and Y. Kawano, "A flexible and wearable terahertz scanner," Nat. Photonics **10**(12), 809–813 (2016).
7. M. Mittendorff, S. Winnerl, and T. E. Murphy, "2D THz Optoelectronics," Adv. Opt. Mater. **9**(3), 2001500 (2021).
8. X. Pang, A. Caballero, A. Dogadaev, V. Arlunno, R. Borkowski, J. S. Pedersen, L. Deng, F. Karinou, F. Roubeau, D. Zibar, X. Yu, and I. T. Monroy, "100 Gbit/s hybrid optical fiber-wireless link in the W-band (75–110 GHz)," Opt. Express **19**(25), 24944–24949 (2011).
9. S. Koenig, D. Lopez-Diaz, J. Antes, F. Boes, R. Henneberger, A. Leuther, A. Tessmann, R. Schmogrow, D. Hillerkuss, R. Palmer, T. Zwick, C. Koos, W. Freude, O. Ambacher, J. Leuthold, and I. Kallfass, "Wireless sub-THz communication system with high data rate," Nat. Photonics **7**(12), 977–981 (2013).
10. X. Yu, S. Jia, H. Hu, M. Galili, T. Morioka, P. U. Jepsen, and L. K. Oxenløwe, "160 Gbit/s photonics wireless transmission in the 300-500 GHz band," APL Photonics **1**(8), 081301 (2016).
11. S. A. Harmon and R. A. Cheville, "Part-per-million gas detection from long-baseline THz spectroscopy," Appl. Phys. Lett. **85**(11), 2128–2130 (2004).
12. N. Nagai, T. Imai, R. Fukasawa, K. Kato, and K. Yamauchi, "Analysis of the intermolecular interaction of nanocomposites by THz spectroscopy," Appl. Phys. Lett. **85**(18), 4010–4012 (2004).
13. Y. Xu and M. Havenith, "Perspective: Watching low-frequency vibrations of water in biomolecular recognition by THz spectroscopy," J. Chem. Phys. **143**(17), 170901 (2015).
14. O. Kojima, Y. Tarui, H. Shimazu, T. Kita, A. Majeed, P. Ivanov, E. Clarke, and R. Hogg, "Wide frequency tuning of continuous terahertz wave generated by difference frequency mixing under exciton-excitation conditions in a GaAs/AlAs multiple quantum well," Phys. Rev. Appl. **10**(4), 044035 (2018).
15. A. Majeed, P. Ivanov, B. Stevens, E. Clarke, I. Butler, D. Childs, O. Kojima, and R. Hogg, "Broadband THz absorption spectrometer based on excitonic nonlinear optical effects," Light: Sci. Appl. **8**(1), 29 (2019).
16. S. Matsuura, M. Tani, and K. Sakai, "Generation of coherent terahertz radiation by photomixing in dipole photoconductive antennas," Appl. Phys. Lett. **70**(5), 559–561 (1997).
17. S. Verghese, K. A. McIntosh, and E. R. Brown, "Optical and terahertz power limits in the low-temperature-grown GaAs photomixers," Appl. Phys. Lett. **71**(19), 2743–2745 (1997).

Optics EXPRESS

18. O. Kojima, T. Isu, J. Ishi-Hayase, A. Kanno, R. Katouf, M. Sasaki, and M. Tsuchiya, "Ultrafast response induced by interference effects between weakly confined exciton states," J. Phys. Soc. Jpn. **77**(4), 044701 (2008).
19. O. Kojima, S. Watanabe, T. Kita, O. Wada, and T. Isu, "Dephasing of excitonic polaritons confined in GaAs thin films," J. Phys. Soc. Jpn. **80**(3), 034704 (2011).
20. G. Bartels, G. C. Cho, T. Dekorsy, H. Kurz, A. Stahl, and K. Köhler, "Coherent signature of differential transmission signals in semiconductors: Theory and experiment," Phys. Rev. B **55**(24), 16404–16413 (1997).
21. O. Kojima, K. Mizoguchi, and M. Nakayama, "Coupling of coherent longitudinal optical phonons to excitonic quantum beats in GaAs/AlAs multiple quantum wells," Phys. Rev. B **68**(15), 155325 (2003).
22. O. Kojima, K. Mizoguchi, and M. Nakayama, "Quantum beats of type-I and type-II excitons in an $In_xGa_1 - xAs$/GaAs strained single quantum well," J. Appl. Phys. **112**(4), 043522 (2012).
23. O. Kojima and T. Kita, "Effects of exciton line widths on the amplitude of quantum beat oscillations," Appl. Phys. Express **9**(6), 062801 (2016).
24. O. Kojima, T. Kita, M. J. Steer, and R. A. Hogg, "Resonant exciton excitation photoluminescence and dynamics in a GaAs/AlAs multiple quantum well with internal electric field," AIP Adv. **10**(9), 095016 (2020).